IOP PUBLISHING PHYSICS IN MEDICINE AND BIOLOGY

Phys. Med. Biol. **54** (2009) 5395–5409 doi:10.1088/0031-9155/54/18/003

The localization of focal heart activity via body surface potential measurements: tests in a heterogeneous torso phantom

F Wetterling[1,2,3,7], M Liehr[1], P Schimpf[4], H Liu[5,6] and J Haueisen[1,2]

[1] Biomagnetic Center, Department of Neurology, Friedrich Schiller University Jena, Jena, Germany
[2] Institute of Biomedical Engineering and Informatics, Technical University of Ilmenau, Ilmenau, Germany
[3] School of Physics, Trinity College Dublin, Dublin, Ireland
[4] Department of Computer Science, Eastern Washington University, Cheney, WA, USA
[5] Massachusetts General Hospital, Massachusetts Institute of Technology and Harvard Medical School, Boston, MA, USA
[6] Athinoula A Martinos Center for Biomedical Imaging, Charlestown, MA, USA

E-mail: wetterlf@tcd.ie

Received 13 February 2009, in final form 31 July 2009
Published 21 August 2009
Online at stacks.iop.org/PMB/54/5395

Abstract

The non-invasive localization of focal heart activity via body surface potential measurements (BSPM) could greatly benefit the understanding and treatment of arrhythmic heart diseases. However, the *in vivo* validation of source localization algorithms is rather difficult with currently available measurement techniques. In this study, we used a physical torso phantom composed of different conductive compartments and seven dipoles, which were placed in the anatomical position of the human heart in order to assess the performance of the Recursively Applied and Projected Multiple Signal Classification (RAP-MUSIC) algorithm. Electric potentials were measured on the torso surface for single dipoles with and without further uncorrelated or correlated dipole activity. The localization error averaged 11 ± 5 mm over 22 dipoles, which shows the ability of RAP-MUSIC to distinguish an uncorrelated dipole from surrounding sources activity. For the first time, real computational modelling errors could be included within the validation procedure due to the physically modelled heterogeneities. In conclusion, the introduced heterogeneous torso phantom can be used to validate state-of-the-art algorithms under nearly realistic measurement conditions.

[7] Author to whom any correspondence should be addressed.

1. Introduction

Source localization is a widely used method to reconstruct the location, orientation and strength of bioelectrical sources from surface potential measurements. The localization of focal heart activity from body surface potential measurements (BSPM) could serve for the accurate diagnosis of pathological heart diseases. Recently, for example, electrocardiographic imaging (ECGI) methods have been proposed for patients with and without risk of life-threatening cardiac arrhythmia (Ramanathan *et al* 2004). Based on those computations, one could determine the cardiac location of the arrhythmic heart region for optimal localized intervention, evaluate the efficacy and guidance of therapy over time and study the mechanisms and properties of cardiac arrhythmias in humans.

To perform source localization, the bioelectrical inverse problem must be solved. The bioelectrical inverse problem formulates the query about the particular source parameters which generate a particular measured field (Sarvas 1987). In general, it is an ill-posed problem, since an infinite number of solutions can be found which account for the measurements. Thus, to arrive at a unique solution, *a priori* information must be included defining the source model and the source space. The source model considers a pool of activated cells *a priori* as an equivalent current dipole and the amount of possible source positions within the source space is *a priori* restricted to an anatomically and physiologically reasonable volume.

In the current study, the Recursively Applied and Projected Multiple Signal Classification (RAP-MUSIC) algorithm was chosen to localize various dipole sets in a heterogeneous torso phantom. The reasons were twofold. Firstly, RAP-MUSIC computes the source parameters from temporally consecutive, spatially resolved surface potential measurements (spatio-temporal approach), which seems to be an adequate approach to reduce zero-mean noise influences on the source localization accuracy. Secondly, the surface potentials are assumed to be generated by a certain number of dipoles which are fixed in orientation and position over the chosen time range. Thus using RAP-MUSIC, a multiple-dipole problem can be split into multiple single-dipole problems, when all dipoles possess temporally independent activity (uncorrelated dipoles). That reduces the generally high complexity of the inverse problem.

By employing the independent topography (IT) approach, the RAP-MUSIC algorithm was specifically designed to localize sources in the presence of further uncorrelated activity that can be composed of self-correlated dipole sets (correlated dipoles/distributed sources) (Mosher and Leahy 1999). Hence, RAP-MUSIC may be applicable to localize focal sources in the presence of distributed heart activity, such as occurring during pathological cardiac arrhythmia.

Validation studies for multiple source localization with RAP-MUSIC were successfully carried out by Ermer *et al* on a *post-mortem* skull localizing two uncorrelated dipoles (Ermer *et al* 2000), by Chang *et al* on two uncorrelated focal sources in a computer simulation study (Chang *et al* 2004) and by Mosher *et al* on three uncorrelated dipoles simulated in a spherical head geometry (Mosher and Leahy 1999). *In vivo* studies showed difficulties in assessing the localization accuracy of the ECGI method, because the human protocol hindered simultaneous measurements of surface potentials and intraoperative potential maps (Ghanem *et al* 2005). However, no phantom study has yet been carried out to investigate the performance of RAP-MUSIC in cases of one uncorrelated dipole in the presence of correlated dipole activity; nor was such a cardiac setup realistically modelled using a heterogeneous volume conductor up to date.

The aim of this study was to analyse the localization accuracy of RAP-MUSIC for single dipoles, two dipoles and three dipoles. These configurations were chosen to clarify robustness of the RAP-MUSIC algorithm when used to localize an uncorrelated dipole in different

cases of accompanying sources activity (no dipole, one dipole, two correlated dipoles). To accomplish this goal, measurements were performed on a custom-built and previously used *anthropomorphic* torso phantom (Tenner *et al* 1999). The phantom was equipped with seven current dipoles and compartments resembling both the lungs and the muscle compartments; such phantom measurements allowed one to consider the influence of real-world factors, while a precise statement on the achieved localization accuracy was possible.

2. Methods

2.1. Torso phantom and dipole sources

A human-shaped torso phantom built from resin with glass fibre was used as a physical model. For electrical data acquisition, 138 Ag/AgCl electrodes were embedded on the surface of the phantom shown in figure 1(a). The phantom was filled with a NaCl solution which had a conductivity of 0.335 S m^{-1} to mimic physiological conductivity (Geddes and Baker 1967, Foster and Schwan 1989). An opening in the abdomen region served to fill the torso with a NaCl solution, to insert additional compartments and to insert and fix the dipolar sources inside. To account for the human electrical properties of tissue being heterogeneous, lungs and muscle compartments were physically modelled with their respective electric properties and geometric dimensions as well. The artificial lungs were modelled as two cylinders (figure 1(c)). The cylinders consisted of a plastic rack covered with ionic exchange membranes ('NEOSEPTA' type CM-2, NISSHO IWAI Deutschland GmbH, Düsseldorf, Germany). The specific property of the ionic membrane was to separate two differently concentrated NaCl solutions from each other but allow ions to pass through when driven by an electrical force. The artificial muscles (figure 1(b)) were composed of six rectangular and curved racks to fit to the inner chest shape of the phantom. Each rack was then plugged into an artificial chest bone, which was screwed on the inner phantom chest surface. The lung conductivity was set to 0.0667 S m^{-1} in order to obtain a conductivity ratio between thorax and lung of approximately 5:1 (Jorgenson *et al* 1995, Czapski *et al* 1996), and the muscle conductivity used was 0.143 S m^{-1} (Ramon *et al* 2002, Foster and Schwan 1989). All saline solutions conductivities were checked with a conductivity meter LF 340 (WTW Wissenschaftlich-Technische Werkstätten GmbH, Weilheim, Germany). The dipoles and the artificial lung model could be positioned precisely and reproducibly by sliding the module into a holder. Two twisted copper wires were used to connect each dipole with the current source (figures 1(d) and (e)). The current source provided 12 output channels, where each channel was galvanically isolated from others. The platinum dipole ends (4 mm length) were soldered on to the copper wire. Only 2 mm of the platinum dipole ends were left blank, whereas the rest of the dipole was insulated by a layer of epoxy resin. The total length of each dipole was 10 mm, resulting in a dipole moment of 15 μA m when supplied by a maximum magnitude of 1.5 mA. Seven of those single dipoles were situated on a rod, which was used to set up several configurations. Each dipole (numbers 1 to 7) could be used in isolation or in combination with others.

The localization accuracy was analysed on different source quantities and configurations. For single dipoles, each of the seven dipoles was used separately, leading to seven configurations. For two uncorrelated dipoles, dipole 7 was always used together with one of the other six dipoles, leading to six configurations. In this manner, the influence of dipole separation on the accuracy could be assessed. The uncorrelated case was set up by feeding dipole 7 with 30 Hz and the accompanying dipole with 20 Hz. The three-dipole configurations were composed of one uncorrelated dipole in conjunction with a correlated dipole pair using dipoles 1, 4 and 7 throughout those. By variation of the uncorrelated dipole's position, three

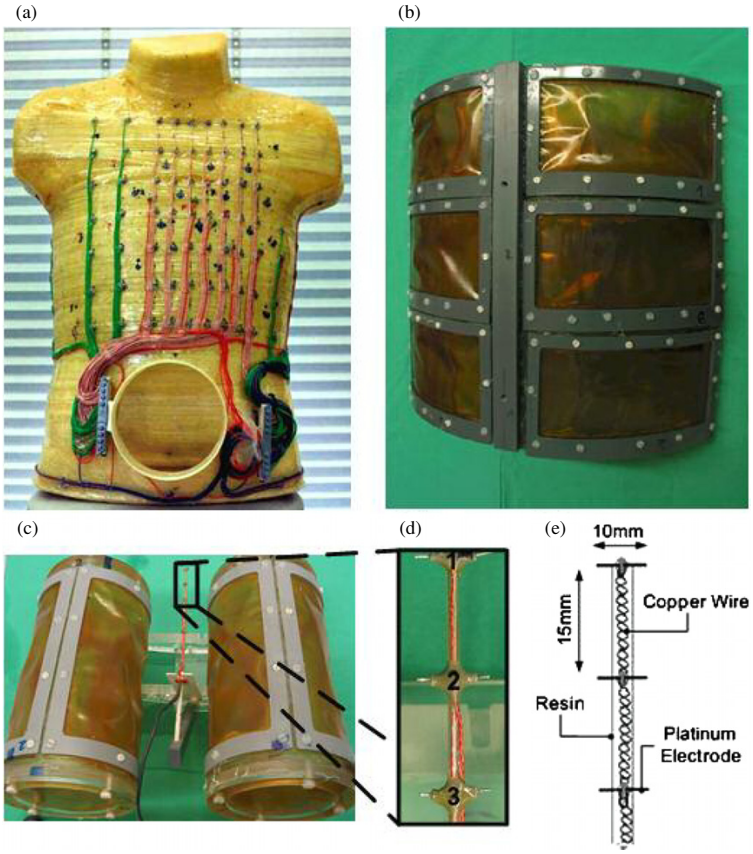

Figure 1. The heterogeneous physical torso phantom and the seven dipolar sources. (a) The human-shaped torso phantom shown from the front with wired electrodes on the chest and a hole beneath, which gave interior access. (b) The muscle compartment composed of six chambers connected to an artificial chest bone. (c) The lung compartments, cylindrical in shape were placed on the piacryle module which was fixed on the inner backside of the torso phantom. (d) The seven dipoles were placed between the lung compartments. Dipole numbers 1 to 3 of the seven dipoles used, each composed of two platinum wires connected with the current source through a twisted copper wire (e). The supply wires were insulated by an epoxy resin coating.

configurations were set up. The influence of differently positioned correlated dipoles on the localization accuracy of the uncorrelated dipole could thus be tested.

2.2. The volume conductor model

The boundary element method (BEM) was chosen to numerically solve the forward problem, i.e. to calculate the potentials given by the sources. The necessary geometrical information was acquired from an x-ray computed tomography (CT) scan (SOMATOM, Siemens, Erlangen, Germany) at the University Hospital Jena, Germany, resolving a voxel size of 1.95 mm $\times$

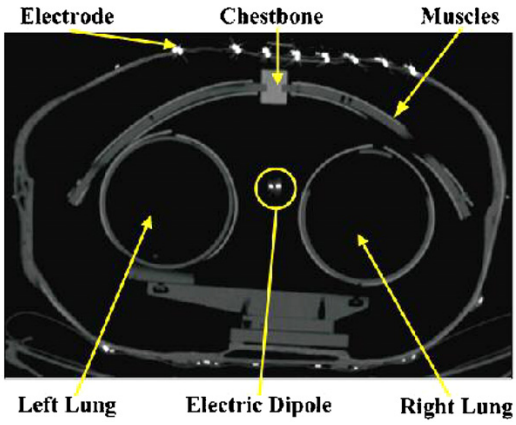

Figure 2. An axial CT-slice through the phantom's setup showing the lung and muscle compartments, as well as one line of the electrode array and one electric dipole.

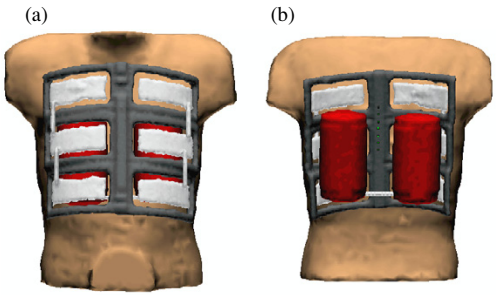

Figure 3. The BEM model in front (a) and rear (b) view. The muscles were modelled as two compartments: one compartment resembling the saline solution (white) and one resembling the plastic frame (grey). The lungs were modelled as one compartment resembling the saline solution (red) under negligence of the plastic frame conductivity.

1.95 mm × 3.9 mm. Figure 2 shows an axial CT-slice through the phantom's setup. The different compartments were then segmented employing the CURRY® software (version 4.51, Compumedics NeuroScan Inc., El Paso, TX, USA). Within each compartment, the conductivity was assumed to be isotropic and ohmic, so that the BEM could be used to solve the forward problem. This required the discretization of boundaries between compartments. The used BEM model is shown in figure 3. The modelling of the muscles and lung compartments was aggravated because of the physically employed plastic frames. The BEM required each compartment to be fully nested and compartment boundaries to be in certain distances. Thus, modelling the plastic frame of the muscle compartment was degraded by the introduction of an artificial gap in between the physical muscle compartment and the plastic frame. At the same time it proved impractical to model the delicate lung plastic frame of 2 mm width as a separate compartment. These facts have to be considered when the localization error is analysed for

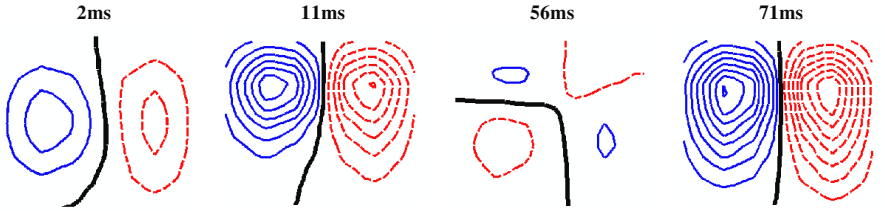

Figure 4. Characteristic surface potential measurements at different time points for two uncorrelated dipoles, dipole 1 and dipole 7 fed with sinusoidal currents (frequencies 20 Hz and 30 Hz, respectively). The contour line increment is 0.5 mV for the surface potential measurement. Solid lines indicate positive values and dashed lines indicate negative values, while the thick line represents the zero potential line. The measurement at 2 ms represents activity of dipole 7 only, at 11 ms activity of dipole 1 only, at 56 ms simultaneous activity of both dipoles with reversed orientations, and at 71 ms simultaneous activity of both dipoles with identical orientations. Differences between the signal magnitudes were due to differently deep positioned dipoles with respect to the electrode array.

Table 1. The BEM model parameters used.

Compartment	Number of triangles	Side length (mm)
Torso	8710	12
Right lung	2036	8
Left lung	2024	8
Plastic frame	9896	4
Muscles	7684	4

dipoles with various distances to the muscle and lung compartments. The number of discrete element triangles and chosen elements side lengths are summarized in table 1.

2.3. Measurements

Measurements were taken in a magnetically shielded room (AtB srl, Pescara, Italy) at the Biomagnetic Center at the Friedrich-Schiller University, Jena, Germany. The electrical data were acquired from 55 electrodes distributed according to the NEMY standard (Hoekema *et al* 1995) on the anterior part of the phantom. The measurement of posterior surface potentials could be neglected for this study due to the known longitudinally arranged dipole sets.

The signal was recorded with a sampling rate of 1025 Hz using electric channels, which had a 256 Hz low-pass filter and were dc coupled with an offset compensation mechanism. Offline, the measurements were baseline-corrected and no additional filtering or averaging was applied. For source localization, a 100 ms data range was chosen from the centre of the 10 s long data set to avoid filtering affected signal distortions. Representative surface potentials for two uncorrelated dipoles are shown in figure 4. The maximum noise magnitude in all configurations was contributed by the 50 Hz noise. Other noise sources were successfully reduced through the shielding chamber.

The signal-to-noise ratio (SNR) was computed as

$$\mathrm{SNR} = 10 \log \left[\frac{\sum_{m=1}^{55} (P_{20\mathrm{Hz}} + P_{30\mathrm{Hz}})_m}{\sum_{m=1}^{55} (P_{50\mathrm{Hz}})_m} \right] \tag{1}$$

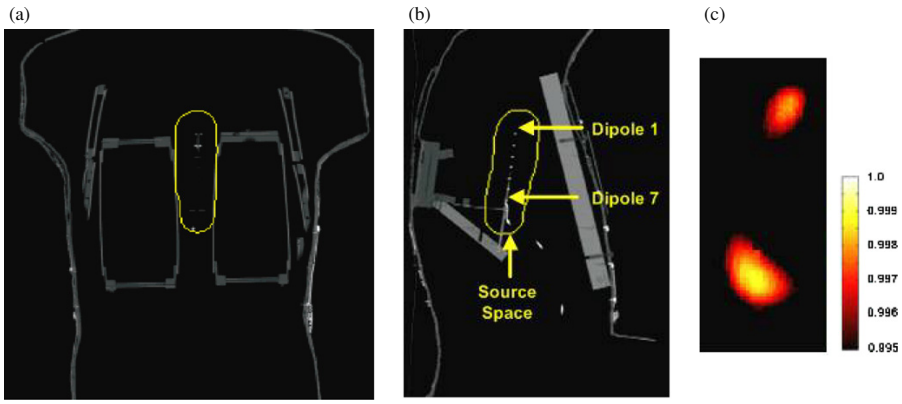

Figure 5. The source space framed with a yellow line comprises the region of possibly reconstructable dipole sources. The results below are represented in the same (a) coronal and (b) sagittal slices, but zoomed into the region of the source space. (c) The subspace correlation spectrum for two uncorrelated dipoles 1 and 7 plotted into the sagittal slice of source space. The local maximum for dipole 7 was wider spread than for dipole 1 due to its deeper position inside the phantom.

where $P_{20\mathrm{Hz}}$ and $P_{30\mathrm{Hz}}$ were the signal power magnitudes and $P_{50\mathrm{Hz}}$ was the noise power amplitude for the mth electrodes channel. The SNR was better than 20 dB for all 16 dipole configurations.

2.4. The source space

Synchronously activated cells in one area were modelled by one equivalent current dipole under the assumption that the distance between the sensors and the source was large compared to the dimensions of the source. A linear relationship between that dipole model and the surface recordings was obtained through a grid definition, where p grid points represented possible source positions within the volume conductor. In our current study the source space was chosen to contain 12 013 grid points around the true dipole positions with a resolution of 1.95 mm × 1.95 mm × 3.9 mm forming a tube-equivalent volume as shown in figure 5. The forward solution explaining the measurements can then be expressed by

$$\overset{m\times n}{V} = \left(\overset{m\times 3p}{L} + \overset{m\times 3p}{E_L}\right) \cdot \overset{3p\times n}{S} + \overset{m\times n}{E_N} \tag{2}$$

where the first column of the $m \times 3p$ Leadfield matrix $\boldsymbol{L}$ represents the potential at the m electrodes due to a dipole source at location 1 in this grid, having unity moment in the x-direction. Similarly, the second and third columns represent the potential due to source 1 with unity moment in the y- and z-direction, respectively. In a physical sense, $\boldsymbol{L}$ represents the material and geometrical properties of the medium in which the sources are submerged (Van Veen *et al* 1997). Furthermore, $\boldsymbol{V}$ denotes the $m \times n$ spatio-temporal matrix composed of the potentials measured at m electrode sites and n time samples.

Finally, $\boldsymbol{S}$ is defined as the $3p \times n$ source matrix containing the x-, y-, z-components of the dipole moment in each grid point with variable activity over n samples in time.

Deviations between model and measurement, which originates from Leadfield matrix errors and superimposed noise, were considered by error matrices $\boldsymbol{E}_L$ and $\boldsymbol{E}_N$.

2.5. Spatio-temporal dipole localization

The RAP-MUSIC algorithm proposed by Mosher and Leahy (1999) uses a spatio-temporal independent topography (IT) model of the source space, whereby an IT is defined as one or more non-rotating dipoles with a single time series. Each IT is spatially and temporally independent of other ITs. In this framework, spatially distinct sources with a synchronous activation comprise a single IT. RAP-MUSIC computes one IT for the maximum subspace correlation value, which is a measure of coincidence between the modelled and the measured surface potentials. Further ITs are computed in an iterative manner by suppressing already computed source positions. A subspace correlation threshold below which sources were not processed anymore must be set. The threshold served as a criterion to decide for the following cases: all dipoles were computed or the IT model order was chosen too low. That allowed the localization of correlated dipole sources, when for instance a single dipole model was insufficiently fit to the surface potentials generated by two correlated dipoles or a distributed source. In this study, the subspace correlation threshold was set to 95%, as recommended by Mosher and Leahy (1998). The signal subspace rank which equals the number of ITs by definition was set 3 for all 16 configurations, as over-specifying the true rank by a couple of dimensions usually has little effect on performance (Mosher and Leahy 1998). Figure 5(c) shows an example of the subspace correlation spectrum for a sagittal slice of source space. The maxima were related to the source positions of temporally uncorrelated dipoles 1 and 7. All dipole sources were localized with the RAP-MUSIC algorithm using a program written in MATLAB® (version 6.5, The MathWorks Inc. Natick, MA, USA). An extensive description of the algorithm itself is provided elsewhere (Mosher and Leahy 1999).

3. Results

To assess the localization accuracy of the RAP-MUSIC algorithm, the localization error in position, angle and subspace correlation was computed for 22 uncorrelated dipoles in 16 configurations. To give the reader a qualitative feeling for the localization error in position, it was also marked as a circled cross in the sagittal and coronal CT images. The angular deviation of the localized dipole moment, the positioning error and the subspace correlation value are listed beside each computed dipole and a summary of the quantitative results can be found in table 2.

3.1. Single dipoles

First, all seven dipoles were activated separately (single dipoles), the surface potentials were measured and their positions were localized. For the discussion below, the dipoles were grouped into dipoles that were close to the lung plastic racks (dipoles 1 and 3) and those that were midway between the two lung compartments (dipoles 4 to 7) as shown in figure 6.

The localization error for all seven single sources averaged 6 $\pm$ 2 mm (mean $\pm$ standard deviation). A shift of the individual dipoles parallel to the dipole rod (coronal view) could be observed. Dipoles 1 to 3 showed an increased error in depth (sagittal slice) relative to the others. These dipoles indicated a lower subspace correlation for the best fitting source model, which was likely due to an oversimplified compartment model nearby. In addition, dipoles 2 and 3 also showed a larger angular deviation from the true dipole moments.

Table 2. Localization results for dipoles 1 to 7 as computed from measured sets of single, two and three dipoles.

Set	Analysed dipole	Accompanying dipoles	Localization error (mm)	Angular error (°)	Subspace correlation (%)	Grid error (mm)
One dipole	1 (20 Hz)	–	10.5	0.1	99.80	2.0
	2 (20 Hz)	–	7.0	12	99.78	1.9
	3 (20 Hz)	–	6.1	13.7	99.76	0.0
	4 (20 Hz)	–	5.6	0.1	99.82	2.7
	5 (20 Hz)	–	2.8	0.1	99.87	0.1
	6 (20 Hz)	–	5.9	0	99.89	1.9
	7 (20 Hz)	–	5.6	0	99.90	3.9
	Mean ± STD		6.2 ± 2.3			1.8 ± 1.4
Two dipoles	1 (20 Hz)	7 (30 Hz)	16.2	49.4	99.78	
	2 (20 Hz)	7 (30 Hz)	20.5	18.1	99.76	
	3 (20 Hz)	7 (30 Hz)	16.7	12.1	99.60	
	4 (20 Hz)	7 (30 Hz)	12.5	20.3	99.70	
	5 (20 Hz)	7 (30 Hz)	11.6	4.1	99.78	
	6 (20 Hz)	7 (30 Hz)	15.8	5.1	99.72	
	Mean ± STD		15.6 ± 3.2			
Two dipoles	7 (30 Hz)	1 (20 Hz)	5.5	4.9	99.90	
	7 (30 Hz)	2 (20 Hz)	8.9	3.6	99.91	
	7 (30 Hz)	3 (20 Hz)	8.9	2.3	99.92	
	7 (30 Hz)	4 (20 Hz)	12.5	22.2	99.92	
	7 (30 Hz)	5 (20 Hz)	12.0	0.8	99.90	
	7 (30 Hz)	6 (20 Hz)	18.0	4.4	99.91	
	Mean ± STD		11.0 ± 4.3			
Three dipoles	1 (20 Hz)	4 and 7 (30 Hz)	11.5	39.7	99.82	
	4 (20 Hz)	1 and 7 (30 Hz)	15.0	13.2	99.99	
	7 (20 Hz)	1 and 4 (30 Hz)	6.4	3.6	99.92	
	Mean ± STD		11.0 ± 4.3			

3.2. Two dipoles

In a second experiment the ability of RAP-MUSIC to localize two uncorrelated dipoles was tested. Dipole 7 (30 Hz) was used in conjunction with dipoles 1 to 6 (20 Hz) yielding six different configurations, where configuration 1 was established by the combination of dipole 1 and dipole 7, configuration 2 by dipole 2 and dipole 7, and so forth. Thus, configuration 1 represented the maximal separation between dipoles and configuration 6 the minimal separation. The localization error for dipole 7, which was used throughout, rose with the proximity of the two dipoles (figure 7). For configuration 6 the estimated error was greater than the dipole separation. The estimated localization error for dipole 7 in the six configurations averaged 11 ± 4 mm (mean ± standard deviation). In addition, the qualitative representation (figure 8) reveals a systematic error. The two dipoles were localized with an overestimated dipole-to-dipole distance, which increased with decreasing dipole separation.

3.3. Three dipoles

Finally, three configurations were set up using three dipoles (1, 4 and 7) to model distributed heart activity by two correlated dipoles and a focal source by one uncorrelated dipole. The qualitative localization results are illustrated in figure 8. The localization error for the

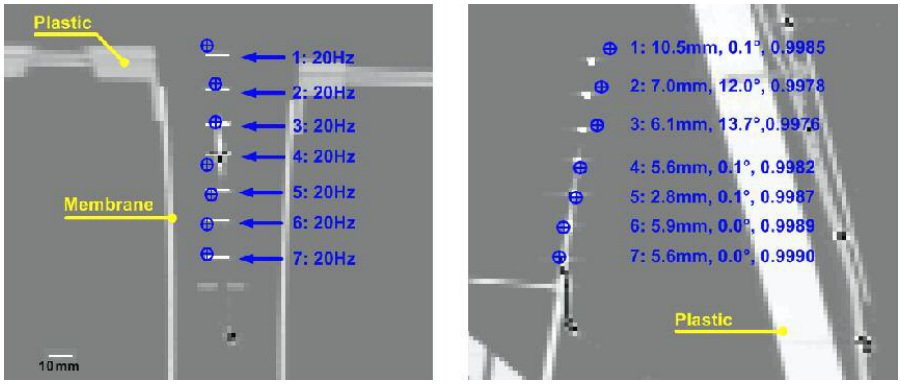

Figure 6. The localization result for seven single dipoles, of which each was switched on and off one after the other. The localized dipole positions were plotted into the x-ray CT images (left: coronal slices; right: sagittal slice). Crossed circles indicate the computed position and arrows point to the activated dipole. The localization error for dipoles 1 to 3 was primarily a depth error. The plastic frame and the membrane of the lung compartments are labelled in the coronol image. The plastic bar on which the muscle compartments were plugged is labelled in the sagittal image. The quantitative results of positioning error, angular deviation and subspace correlation are listed next to each dipole.

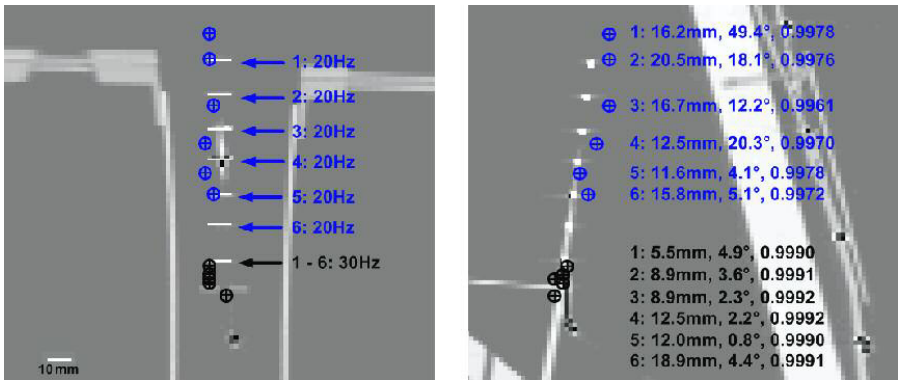

Figure 7. The localization error for six configurations of two uncorrelated dipoles (left: coronal slices; right: sagittal slice). The localization error for dipole 7 (black markers) increased with dipole proximity.

uncorrelated dipole was 11 ± 4 mm (mean $\pm$ standard deviation). The threshold was initially set to 0.95. In order to achieve a two-source IT model for the correlated pair, a threshold of 0.9983 was required. Hence, no two dipoles were computed and instead only one dipole was fit to the manifold of the correlated dipole pair.

4. Discussion

The localization accuracy of the RAP-MUSIC algorithm was tested on 16 dipole configurations of one, two and three activated dipoles in a physical torso phantom, modelling focal and distributed heart activity in a human torso.

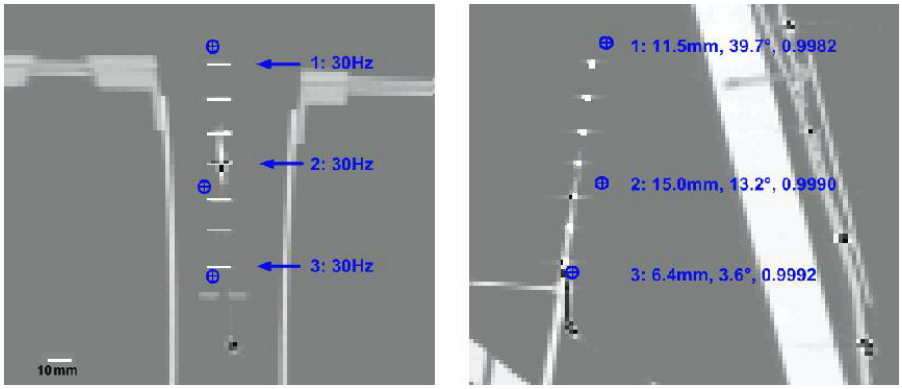

Figure 8. The localization errors for three single dipoles (positions shown), which were accompanied by a pair of two correlated dipoles (left: coronal slices; right: sagittal slice).

4.1. The localization accuracy for single dipoles in a heterogeneous phantom

The localized single dipoles were all allocated to the physically activated dipole, confirming the ability of RAP-MUSIC to localize dipoles in the depth of the human heart muscle, via BSPM. The localization accuracy found for single dipoles was 6 ± 2 mm. Studies using the same phantom without muscle compartments found slightly better accuracies of 5 ± 2 mm (Tenner *et al* 1999, Liehr *et al* 2005). Studies that have localized single dipoles in the same phantom without any other compartment indicated localization accuracies of 4 ± 2 mm (Tenner 2001), and better than 3 mm (Liehr *et al* 2005). The estimated localization error in our study therefore appears reasonable compared to homogeneous volume conductor studies. Other studies which used physiological components to physically model the volume conductor yielded increased localization errors when using the boundary element method (BEM). The localization accuracy for paced sites on dog heart in a homogeneous human torso-shaped tank was found to be better than 10 mm (Oster *et al* 1997). The localization of single dipoles in a post-mortem human skull yields no better accuracies than 8 mm (Leahy *et al* 1998) and 12.5 mm (Baillet *et al* 2001).

In this study, the localization accuracy was influenced by a shift in the compartments and dipole positions during phantom preparation, when the phantom was filled with a fresh NaCl solution. The CT scan was carried out with no filled compartments for better image contrast. The 3D replacement error resulted in an offset of all seven dipoles to the left, as can be observed in figure 6 (coronal slice). Further errors were caused by the fixed grid resolution of 1.95 mm × 1.95 mm × 3.9 mm, whereby possible grid points were not necessarily aligned with the true activated dipole positions.

The closest grid point position for every dipole was plotted in figure 9 to demonstrate the inherent gridding error. The electrodes, dipoles and compartment coordinates were acquired from one CT scan. Therefore, the corregistration error depended solely on the image data resolution was 1.95 mm × 1.95 mm × 3.9 mm.

4.2. The influence of the BEM on the localization accuracy

The deficits of the BEM will be discussed on the increased error of single dipoles 1, 2 and 3. These dipoles were positioned in near proximity to the artificial lung's plastic rack, which was

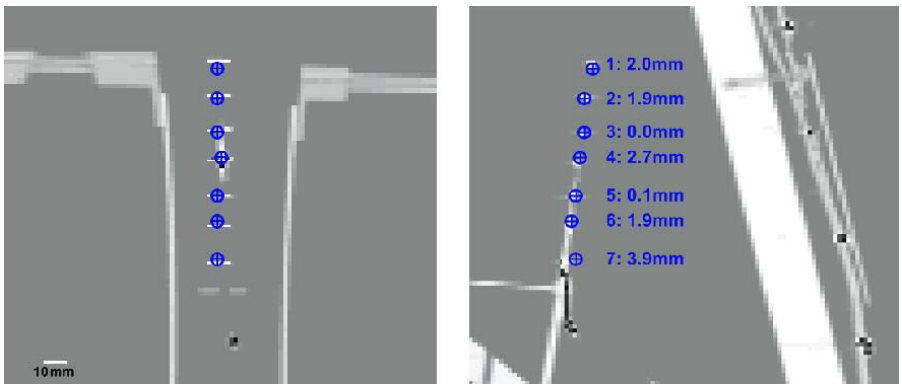

Figure 9. The inherent grid error computed as the nearest grid point (blue) to each of the seven dipole sources (white sticks). The values in mm indicate the 3D difference between the physical dipole position and the closest grid point of the source space (left: coronal slices; right: sagittal slice).

too small to be modelled using the BEM. A major problem of the BEM is that each compartment must be completely nested in another compartment. Consequently shared boundaries between more than two compartments were impossible to be modelled. It appeared as if such small compartments influenced the localization error severely, when closely positioned to the source and when its conductivity was inadequately modelled. This was also tested by Dutz *et al* (2006), who found increased localization errors for BEM models with more than five times under- or overestimated compartment conductivities. Although better discretization of the boundary elements could improve the source localization accuracy, the BEM suffers from the incapability to model compartments with more than two shared boundaries. Hence, for data analysis of body surface potential measurements, more complex forward models based e.g. on the finite element method (FEM) are expected to yield superior results.

As a measure of the BEM model inaccuracy, a Leadfield matrix error was introduced in equation (2), which represented the generally unknown deviation between measured and computed potential distribution for a particular dipole position, and the BEM model. The phantom setup allowed for measuring the selected Leadfield matrix errors corresponding to the seven installed dipole positions. On that basis, the BEM model was changed and the forward modelling error was minimized. For example, the muscle compartment was initially modelled as one entity of muscular conductivity omitting the low conductivity of the plastic skeleton. After separating the compartment into two, one assigned with plastic skeleton and the other with saline conductivity, the localization error for dipoles 1 to 6 was reduced by up to 40% depending on the dipole's distance from the muscle structure.

Forward modelling errors were mostly not considered in computer simulation studies, which generally used identical and therefore errorless forward solutions for the simulation and the localization process. Consequently, such studies showed excellent source localization results for sets of uncorrelated dipole and noise sources. Simulation studies gained localization results with an accuracy of the source space's grid resolution, e.g. 1 mm for a 1.5 mm spaced grid (Mosher and Leahy 1999).

As opposed to the cerebral volume conductor, the torso volume conductor changes continuously over time when the heart muscle moves and the subject breaths. Therefore,

it would be desirable to measure surface potentials and anatomical data sets simultaneously. Corresponding volume conductor models for each surface potential measurement ought then to be generated. Even though model changes with time were not considered in our current torso experiments, we conclude that inadequately modelled lung and heart volumes may cause increased localization errors as observed for dipoles which lay nearby the lung's plastic racks.

4.3. Two dipoles

Analysing the localization error for a dipole accompanied by another uncorrelated dipole shows no significant increase in localization error for dipoles which were neither influenced by forward modelling errors nor too little separated from the accompanying dipole. This was measured in six configurations where two uncorrelated dipoles were localized after varying their spatial separation. Dipole 7, the dipole which was presumably the least influenced by BEM model inaccuracies, was used throughout all six configurations and each of the other six dipoles was switched on and off one after the other. Thus the localization error of dipole 7 served as a quantitative indication of spatial separation on the localization error, which increased from 6 to 19 mm with decreasing dipole separation (dipoles 1 to 6). That indicated a severe influence of spatial separation. The dipole–electrodes distance (90 to 130 mm) and the electrodes' coverage on the torso surface may have hindered the resolution of so closely placed dipoles. A qualitative analysis of the reconstructed positions showed that the separation between the dipoles was always overestimated. This overestimation represents the largest contribution to the position error. The best confirmation of that effect was visible for the sixth configuration of very closely placed dipoles 6 and 7, which were only separated by 15 mm, less than the localization error for this setup (figure 7). Also Liehr *et al* had difficulties to resolve dipoles with less than 30 mm separation using a similar measurement setup (Liehr *et al* 2005).

4.4. Three dipoles

The last experiment included three configurations of one uncorrelated dipole accompanied by two correlated dipoles, always using dipoles 1, 4 and 7, but varying the uncorrelated dipole's positions. These mixed configurations served as a model for pathological focal and normal distributed heart activity. Comparing the localization error of the uncorrelated dipole with its single dipole error, only a slight increase of positioning error ($\sim$1 mm) was found for dipoles 1 and 7. However, the localization error for dipole 4 was more than doubled from 5.6 mm to 15.0 mm. This may be explained by its position midway between the correlated dipole pair. The best fitting single dipole for the two correlated dipoles would have been closely placed to dipole 4, approximately in dipole 3. Thus an identical effect as previously observed for two closely placed uncorrelated dipoles may have caused the increased localization error in this special case. Nevertheless, RAP-MUSIC localized the uncorrelated dipole close to the activated dipole positions for all three cases.

4.5. RAP-MUSIC

The RAP-MUSIC algorithm proved useful for the localization of uncorrelated dipoles in configurations of up to three dipoles. The algorithm relies on a subspace threshold, which is an important selection criterion for the acceptation or rejection of localized dipole parameters. It was set to a constant value of 95% for all configurations, as recommended for neuronal dipole source localization (Mosher and Leahy 1998). Yet, the computed subspace correlation

for the best fitting single dipole to a correlated dipole pair was as high as 99.8%. Thus, a threshold of 95% may not be appropriate for cardiac source localization. Future studies must investigate the use of an SNR-based threshold for cardiac source localization with RAP-MUSIC as suggested by Katyal *et al* who worked out an SNR-based threshold computation method (Katyal and Schimpf 2004).

A correlation between position error, angular deviation and subspace correlation could not be established for the measured dipole configurations in this study.

4.6. Diagnostic relevance

This study was to investigate the source localization accuracy for a highly optimized dipole localization algorithm under real-world volume conductor influences. Although cardiac conduction is often governed by slow conduction through Ca^{2+} mediated activation, it is assumed that the dipole representation for arrhythmias can be verified in future human experiments.

5. Conclusion

Our study of the source localization performance of RAP-MUSIC using a heterogeneous torso phantom shows the necessity and benefits of such phantom studies to validate state-of-the-art algorithms. In this paper, we used a simple phantom setup and a BEM model to test whether the spatio-temporal RAP-MUSIC algorithm can be used to localize uncorrelated focal heart activity in the human torso when accompanied by correlated dipoles or distributed sources. The localization accuracy decreased in dependence of the dipole quantity and with decreasing dipoles separation. Modelled focal heart activity was localized with an average accuracy of 11.0 ± 4.3 mm. The influence of various forward models and compartment conductivities on the achieved source localization accuracy will be studied in future torso phantom experiments.

Acknowledgments

This work was in part supported by the German Research Foundation (DFG Ha 2899/6-1 & 8-1) and the Thuringian Ministry of Education (2008FE9005).

References

Baillet S, Riera J J, Marin G, Mangin J F, Aubert J and Garnero L 2001 Evaluation of inverse methods and head models for EEG source localization using a human skull phantom *Phys. Med. Biol* **46** 77–96

Chang N, Gotman J and Gulrajani R 2004 Dipole localization using beamforming and RAP-MUSIC on simulated intracerebral recordings *Conf. Proc. IEEE Eng. Med. Biol. Soc* **2** 1010–3

Czapski P, Ramon C, Huntsman L L, Bardy G H and Kim Y 1996 On the contribution of volume currents to the total magnetic field resulting from the heart excitation process: a simulation study *IEEE Trans. Biomed. Eng.* **43** 95–104

Dutz S, Bellemann M E, Leder U and Haueisen J 2006 Passive vortex currents in magneto- and electrocardiography: comparison of magnetic and electric signal strengths *Phys. Med. Biol.* **51** 145–51

Ermer J J, Mosher J C, Huang M and Leahy R M 2000 Paired MEG data set source localization using recursively applied and projected (RAP) MUSIC *IEEE Trans. Biomed. Eng.* **47** 1248–60

Foster K R and Schwan H P 1989 Dielectric properties of tissues and biological materials: a critical review *Crit. Rev. Biomed. Eng.* **17** 25–104

Geddes L A and Baker L E 1967 The specific resistance of biological material–a compendium of data for the biomedical engineer and physiologist *Med. Biol. Eng.* **5** 271–93

Ghanem R N, Jia P, Ramanathan C, Ryu K, Markowitz A and Rudy Y 2005 Noninvasive electrocardiographic imaging (ECGI): comparison to intraoperative mapping in patients *Heart Rhythm* **2** 339–54

Hoekema R, Huiskamp G J, Oostendorp T F, Uijen G J and Van oosterom A 1995 Lead system transformation for pooling of body surface map data: a surface Laplacian approach *J. Electrocardiol* **28** 344–5

Jorgenson D B, Haynor D R, Bardy G H and Kim Y 1995 Computational studies of transthoracic and transvenous defibrillation in a detailed 3-D human thorax model *IEEE Trans. Biomed. Eng.* **42** 172–84

Katyal B and Schimpf P H 2004 Multiple current dipole estimation in a realistic head model using R-MUSIC *Conf. Proc. IEEE Eng. Med. Biol. Soc.* **2** 829–32

Leahy R M, Mosher J C, Spencer M E, Huang M X and Lewine J D 1998 A study of dipole localization accuracy for MEG and EEG using a human skull phantom *Electroencephalogr. Clin. Neurophysiol.* **107** 159–73

Liehr M, Haueisen J, Goernig M, Seidel P, Nenonen J and Katila T 2005 Vortex shaped current sources in a physical torso phantom *Ann. Biomed. Eng.* **33** 240–7

Mosher J C and Leahy R M 1998 Recursive MUSIC: a framework for EEG and MEG source localization *IEEE Trans. Biomed. Eng.* **45** 1342–54

Mosher J C and Leahy R M 1999 Source localization using recursively applied and projected (RAP) MUSIC *IEEE Trans. Sign. Proc.* **47**

Oster H S, Taccardi B, Lux R L, Ershler P R and Rudy Y 1997 Noninvasive electrocardiographic imaging: reconstruction of epicardial potentials, electrograms, and isochrones and localization of single and multiple electrocardiac events *Circulation* **96** 1012–24

Ramanathan C, Ghanem R N, Jia P, Ryu K and Rudy Y 2004 Noninvasive electrocardiographic imaging for cardiac electrophysiology and arrhythmia *Nat. Med.* **10** 422–8

Ramon C, Schimpf P, Wang Y, Haueisen J and Ishimaru A 2002 The effect of volume currents due to myocardial anisotropy on body surface potentials *Phys. Med. Biol.* **47** 1167–84

Sarvas J 1987 Basic mathematical and electromagnetic concepts of the biomagnetic inverse problem *Phys. Med. Biol.* **32** 11–22

Tenner U 2001 *Source Modeling in Cardiomagnetism: A Physical Torso Phantom for Biomagnetic and Bioelectric Heart Field Measurements* (München: Verlag Dr Hut)

Tenner U, Haueisen J, Nowak H, Leder U and Brauer H 1999 Source localization in an inhomogeneous physical thorax phantom *Phys. Med. Biol.* **44** 1969–81

Van Veen B D, Van Drongelen W, Yuchtman M and Suzuki A 1997 Localization of brain electrical activity via linearly constrained minimum variance spatial filtering *IEEE Trans. Biomed. Eng.* **44** 867–80